Journal of Earthquake Engineering Vol. 2, No. 3 (1998) 443–473

A FIBRE FINITE BEAM ELEMENT WITH SECTION SHEAR MODELLING FOR SEISMIC ANALYSIS OF RC STRUCTURES

GIULIO RANZO
Visiting Research Engineer, University of California San Diego, Department of Applied Mechanics and Engineering Sciences, Structural Systems Research, La Jolla, CA 92093-0085, USA

MARCO PETRANGELI
Research Engineer, Università degli Studi di Roma "La Sapienza", Dipartimento di Ingegneria Strutturale e Geotecnica, Via Eudossiana 18, 00184 Rome, Italy

Received 10 March 1997
Revised 19 September 1997
Accepted 13 October 1997

The paper describes the formulation of a non-linear, two-dimensional beam finite element with bending, shear and axial force interaction for the static and dynamic analysis of reinforced concrete structures. The hysteretic behaviour of "squat" reinforced concrete members, in which the interaction between shear and flexural deformation and capacity is relevant for the overall structural performance, is emphasised. The element is of the distributed inelasticity type; section axial-flexural and shear behaviours are integrated numerically along the element length using a new equilibrium-based approach. At section level a "hybrid" formulation is proposed: the axial-flexural behaviour is obtained using the classic fibre discretisation and the plane sections remaining plane hypothesis, the shear response instead is identified with a non-linear truss model and described with a hysteretic stress-strain relationship. The latter contains a damage parameter, dependent on flexural ductility, that provides interaction between the two deformation mechanisms. The element has been implemented into a general-purpose finite element code, and is particularly suitable for seismic time history analyses of frame structures. Analytical results obtained with the model are compared with recent experimental data.

Keywords: fibre finite elements, shear strength, flexural ductility.

1. Introduction

The shear deformation mode is often ignored in the inelastic time history analyses of reinforced concrete structures. Most of the non-linear finite beam elements available today in literature are not capable of accounting for a realistic shear inelastic response. When the shear span ratio of the analysed members becomes less than about 2, this approximation might cause an incorrect assessment of inelastic deformation distribution through the entire structure. If energy dissipation is only flexural, curvatures tend to be overestimated and eventually the analysis will lead to an unrealistic plastic mechanism.

The need for bending-shear-axial force interaction modelling comes from the demand for reliable predictions of the dynamic response and the failure mechanism of structures composed of both slender and squat members, subjected to seismic actions. Typically, in the seismic analyses of bridge structures, if one of the piers happens to be much shorter than the others, its shear behaviour (including the possibility of failure) needs to be monitored. In order to identify and describe such cases, this paper dedicates particular attention to the shear mechanism and to the influence of the amount of transverse reinforcement on general member behaviour. The importance of the problem is underlined by the attention of recent European and US codes [EC8, 1994; UBC, 1988] for concrete confinement design details. Both in the US and Japan many of the existing bridge structures, designed in accordance to old standards and often very lightly reinforced for shear, performed poorly during the latest seismic events.

The analysis of a large number of experimental data from shear-sensitive structures suggests that the cyclic behaviour of such members is governed not only by the distribution but also by the type of transverse reinforcement (stirrups, hoops, single or interlock spirals), the amount of axial force, and the level as well as the type of damage which develops in both concrete and steel due to associated bending forces. Essentially, the nominal shear strength is reduced by the increase of curvature ductility, while axial load and transverse steel confining pressure delay and control, respectively, the shear cracking development. This conceptual description of the qualitative behaviour was first proposed in 1981 by the Applied Technology Council for bridge piers [ATC-6, 1981]. Referring to a structural member under lateral actions, it was observed that the shear strength decreases linearly with increasing displacement ductility. Although conceptually valuable, this approach was not implemented into design codes, except for ACI 318/89 [1989] in a very simplified form. Recent studies [Priestley *et al.*, 1994], based on an extended database of experimental results on the behaviour of brittle shear bridge test specimens [Priestley *et al.*, 1993], provided a very accurate quantitative description of this phenomenon. In fact, it was found that a linear correlation between concrete contribution to shear strength and displacement (or curvature) ductility matches very well with the experimental results.

The phenomenological interpretation described above has been assumed as a basis to build a bending-shear-axial force interaction model that has been adopted in the finite element presented herein (see Sec. 2). The element theory, briefly discussed in Sec. 3, follows the new equilibrium-based approach presented in Petrangeli and Ciampi [1997]. The element strain state determination is reached with an iterative procedure in which equilibrium along the element is achieved by imposing the strain field compatibility with the assigned nodal displacements. Stress-strain behaviour is monitored at each step in a discrete number of control sections along the beam axis. The numerical integration along the element length is performed using the classic Gauss-Legendre or Gauss-Lobatto formulae.

A comparison of analytical results with experimental data from different types of shear-dominated quasi-static tests shows good agreement in terms of force-displacement hysteresis loops and lateral displacement profiles. A dynamic analysis of a one-storey frame is presented to compare the damage distribution in a redundant structure using the new model and a classical, purely flexural one.

2. Characteristics of the Interaction Model

Since shear strength decay can be attributed to local flexural damage (e.g. curvature ductility), from the modelling standpoint it seemed appropriate to define a section shear constitutive relationship as a function of axial-flexural response. This approach requires the use of a very refined axial flexural model to provide damage indications for shear response. Today, the flexural behaviour of reinforced concrete one-dimensional structures can be accurately modelled with the so called "fibre" beam element [Kaba and Mahin, 1984; Mahasuverachi and Powell, 1982]. In this type of element, the section is divided into small sub-domains where uniaxial stress-strain laws are used to describe the response of concrete and steel in the longitudinal direction (parallel to the beam axis). These models provide an accurate description of the damage history of the section due to axial and bending forces as well as their interaction. Different authors [Bazant and Bhat, 1977; Garstka *et al.*, 1993] have already investigated the possibility of using the fibre approach and extend it so as to include in it the shear modelling, although no such elements are today available (to the writers' knowledge) for computational purposes, except for the work presented in Petrangeli [1996].

In order to effectively implement a finite element with shear capabilities, the classic flexural fibre model and a simple section shear hysteretic model are superposed. The two mechanisms are then coupled by the damage criterion (discussed in Sec. 1) at section level and integrated along the element length (Fig. 1). This procedure avoids the difficult definition of a shear-bending interaction surface, and does not require the framework of the theory of plasticity. A pre-defined ultimate interaction domain for reinforced concrete sections, to be used in a finite beam element, has been proposed in Sfakianakis and Fardis [1991] to study the biaxial flexure – axial force interaction (defined in the M_x-M_y-P space), using the Bounding Surface Plasticity Model [Yang *et al.*, 1985]. This approach could have been extended to the case of uniaxial flexure with shear, using a section ultimate surface defined in the M-P-V space rather than in M_x-M_y-P space. Several examples of these surfaces are given in [Minami and Wakabayashi, 1981]. Nevertheless, this approach has not been followed because of the drawbacks in the numerical implementation for sections of general type, made of different materials. The use of closed form equations for the flexure-shear coupling at section level has therefore been discarded, and a "hybrid" formulation has been adopted instead. The flexural behaviour is represented with a rational model, while shear response is described by an empirical stress-strain relationship calibrated to experimental observations.

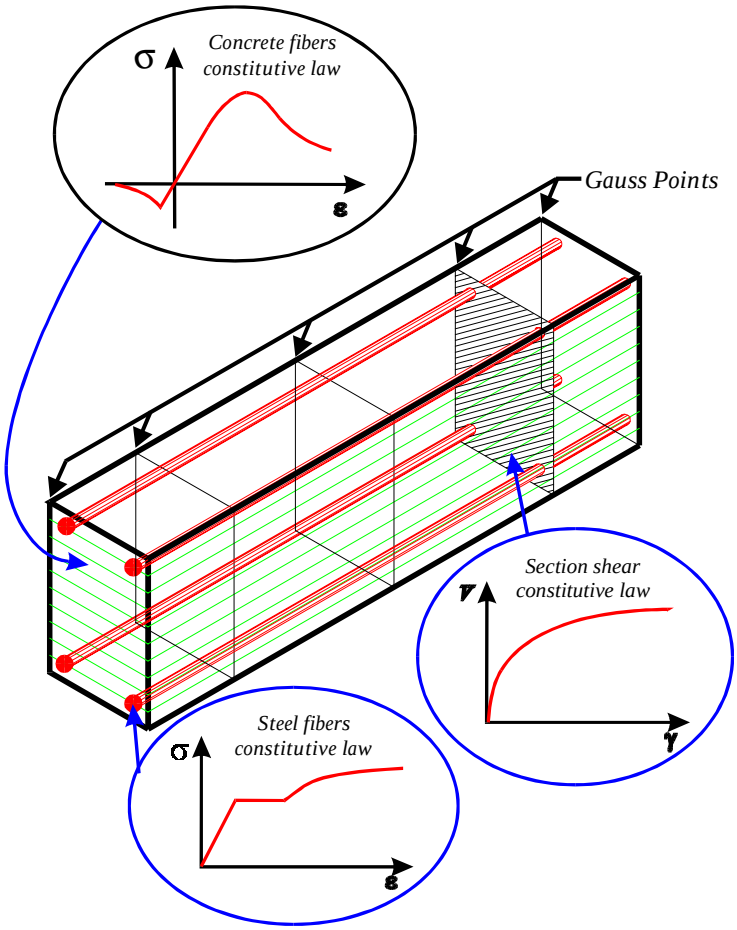

Fig. 1. Element scheme.

The hysteretic model proposed for section shear response is a modified Takeda in which the skeleton branch is a curve that can be scaled depending on the maximum ductility level reached by the section during the analysis. Unloading and reloading branches are linear. The proposed model requires a procedure to define a "*primary* skeleton curve", which describes the section shear force/shear distortion relation under monotonic loading when the ductility dependence is neglected. The response envelope under cyclic loading will then be obtained by letting the primary curve become a function of section ductility by means of section axial deformation.

One option to define the monotonic behaviour is provided by the Compression Field Theory [Collins, 1978], which derives this relation for reinforced concrete beams. Assuming as unknown the angle θ of inclination of the diagonal cracks, equilibrium between the applied shear and the internal resisting forces (developed in concrete and steel reinforcement) can be obtained with an iterative procedure.

If a constant average value of the angle θ is assumed instead (independent on the level of lateral load), the shear force/shear distortion ($V - \gamma$) curve can be defined by solving simple strut-and-tie models. A non-linear truss is proposed herein for such a purpose (Fig. 6).

We assume the section shear behaviour be the same as that of a beam segment of RC beam. The structural mechanism of a generic segment under shear force can be represented with a three chord model: one represents the diagonal concrete compression struts which develop within the segment length, one the concrete struts in tension, and one the segment reinforcement. This procedure allows the determination of the cracking, yielding and ultimate values of shear force and distortion, as a function of cross-section geometry, percentage of transverse reinforcement and axial force level. Once these characteristic points are known, they are interpolated with a simple analytical expression that will be used in the finite element analysis to define the section shear behaviour. Before being implemented, implicit dependence of this curve on the section maximum ductility is introduced. The procedure adopted to define the $V - \gamma$ relation using a non-linear truss model is described in Sec. 4.

3. Element Theory

As mentioned above, section axial-flexural behaviour is a function of section axial deformation (ε) and curvature (χ), as in the traditional fibre model [Kaba and Mahin, 1984], while shear behaviour is a function of section distortion (γ) and of axial deformation (ε):

$$\begin{aligned} M &= M(\chi, \varepsilon) \\ P &= P(\chi, \varepsilon) \\ V &= V(\varepsilon, \gamma) \end{aligned} \tag{1}$$

with the section stress and strain vectors being

$$\boldsymbol{p}(x) = \begin{vmatrix} M \\ P \\ V \end{vmatrix} \quad \boldsymbol{q}(x) = \begin{vmatrix} \chi \\ \varepsilon \\ \gamma \end{vmatrix} , \tag{2}$$

where M is the bending moment, P the axial force and V the shear stress.
The section stiffness matrix can be written as

$$k_s(x) = \begin{bmatrix} k_{11} & k_{22} & 0 \\ k_{21} & k_{22} & 0 \\ 0 & 0 & k_{33} \end{bmatrix} . \tag{3}$$

The terms k_{11}, k_{12}, k_{21}, k_{22} come from the fibre model and are obtained via the integration in the section domain of concrete and steel fibres stiffnesses, determined from uniaxial cyclic constitutive laws [Petrangeli, 1996]. The term k_{33} represents the shear stiffness and is a function of the shear distortion γ and of the discrete

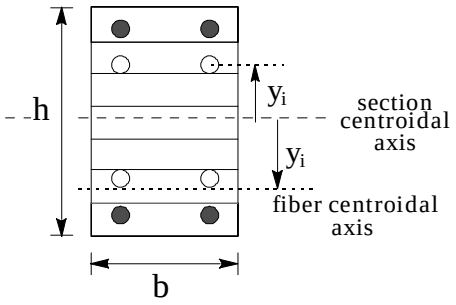

Fig. 2. Fibre model.

variable $\varepsilon_{\max}$, defined as the maximum value of ε which occurs during the analysis (more details are given in Sec. 4). The remaining terms are equal to zero since, as mentioned above, no explicit bending-shear coupling is introduced in the definition of the section stiffness matrix.

The flexural and axial stiffnesses are found in the usual way: the section is divided into n_f fibres, with y_i being the distance from the section centroidal axis to the ith fibre centroidal axis and A_i the area of the fibre. The stiffnesses, referring to Fig. 2, are therefore found as (see Kaba and Mahin [1984] and Petrangeli [1996])

$$k_{11} = \sum_{i=1}^{n_f} A_i E_i y_i^2$$

$$k_{12} = K_{21} = \sum_{i=1}^{n_f} A_i E_i y_i \tag{4}$$

$$k_{22} = \sum_{i=1}^{n_f} A_i E_i$$

in which E_i is the material tangent Young's modulus (steel or concrete, respectively).

The k_{33} term is obtained by considering the current slope of the shear cyclic law (Fig. 8). Details of the equations describing loading, unloading and reloading branches are given in Sec. 5. At this stage we will define k_{33} as

$$k_{33} = \frac{\partial[V(\gamma, \varepsilon_{\max})]}{\partial\gamma}\,, \tag{5}$$

where $V(\gamma, \varepsilon_{\max})$ is the general form of the shear constitutive relationship (including skeleton, unloading and reloading branches, see Fig. 8).

The element formulation follows an equilibrium-based approach [Petrangeli and Ciampi, 1997] within the framework of the displacement method (used by most finite element codes). This particular procedure performs the element state determination

using the "stress shape functions" ($\boldsymbol{b}(x)$), which, for the beam case, are always known and do not depend on the form of the material constitutive relations

$$\begin{cases} M(x) = -(1 - x/L)M_i + \dfrac{x}{L}M_j \\ P(x) = P_j \\ V(x) = \dfrac{M_i + M_j}{L} \end{cases} \qquad \boldsymbol{b}(x) = \begin{bmatrix} -(1-x/L) & x/L & 0 \\ 0 & 0 & 1 \\ 1/L & 1/L & 0 \end{bmatrix}, \tag{6}$$

where M_i and M_j are the end moments and P_j is the axial load. These forces, indicated in the following as vector $\mathbf{P}$, are associated with the element end deformations (φ_i, φ_j and δ), indicated in the following as vector $\mathbf{Q}$. Element degrees of freedom and end forces are shown in Fig. 3, while stress shape functions in Fig. 4.

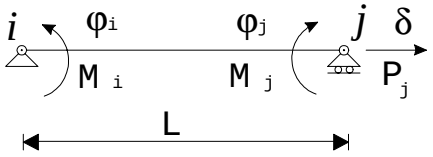

Fig. 3. Element forces and deformations.

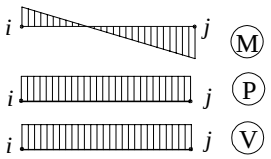

Fig. 4. Stress shape functions.

It has to be noted that the flexibility-based approach, as opposed to the classical stiffness method, is the only viable solution for the implementation of this element. Since curvatures, as well as axial strains and shear distortions, are in general nonlinear along the element length, the stiffness method would require a large number of elements to model a single member. With this approach instead, one element is generally sufficient to model accurately the member behaviour. Further discussion on the advantages of flexibility-based finite element formulation, using stiffness or flexibility-based local stress-strain relations, is given in Spacone *et al.* [1992].

In the element state determination the unknown is the vector of the section strains $\boldsymbol{q}(x)$ of Eq. (2), which will be obtained by the following iterative procedure. A trial element strain field $\boldsymbol{q}(x)$ is modified with homogeneous functions until equilibrium along the element is satisfied. The typical state determination step can be written as follows:

- once nodal deformations Q have been assigned, section deformations are found as

$$\boldsymbol{q}(x) = \alpha(x)\boldsymbol{Q} \tag{7}$$

where $\alpha(x)$ can be any compatible shape function matrix satisfying the following condition:

$$\int \boldsymbol{b}^T(x)\alpha(x)\boldsymbol{b}(x)dx = \boldsymbol{I}\,. \tag{8}$$

The most advantageous formulation can be found by using the section tangent flexibility matrix $\boldsymbol{f}_s(x)$:

$$\alpha(x) = \boldsymbol{f}_s(x)\boldsymbol{b}(x)\boldsymbol{F}^{-1}\,, \tag{9}$$

where $\boldsymbol{F} = \int \boldsymbol{b}^T(x)\boldsymbol{f}_s(x)\boldsymbol{b}(x)dx$ is the element flexibility matrix.

- The section stresses $\boldsymbol{p}(x)$ corresponding to the strain field (7) are then found using the section fibre discretisation and the $V-\gamma$ stress-strain behaviour (1):

$$\boldsymbol{p}(x) = \boldsymbol{p}[\boldsymbol{q}(x)] \tag{10}$$

- The nodal forces P are found with the following integral:

$$\boldsymbol{P} = \boldsymbol{F}^{-1}\int \boldsymbol{b}^T(x)\boldsymbol{f}_s(x)\boldsymbol{p}(x)dx \tag{11}$$

- The umbalance along the element is calculated as follows:

$$\boldsymbol{r}_p(x) = \boldsymbol{b}(x)\boldsymbol{P} - \boldsymbol{p}(x) \tag{12}$$

- A norm of the energy associated with this umbalance is computed as

$$E_{um} = r_p^T(x)\boldsymbol{f}_s(x)\boldsymbol{r}_p(x) \tag{13}$$

- If this energy is less than a specified tolerance, the iterations stop, otherwise a homogeneous strain field correction is found as

$$\boldsymbol{q}_n^*(x) = \boldsymbol{f}_s(x)[\boldsymbol{b}(x)\boldsymbol{P} - \boldsymbol{p}(x)] \tag{14}$$

- The cycle is repeated from step (10) using the new strain field:

$$\boldsymbol{q}^i(x) = \boldsymbol{q}^{i-1}(x) + \boldsymbol{q}_n^*(x) \tag{15}$$

For a finite load step, the above algorithm can therefore be summarised (in the incremental form) as follows:

$$\Delta\boldsymbol{P}^i = \boldsymbol{F}_{i-1}^{-1}\int_0^L \boldsymbol{b}^T(x)\boldsymbol{f}_s^{i-1}(x)\Delta\boldsymbol{p}[\Delta\boldsymbol{q}^{i-1}(x)]dx \tag{16}$$

$$\Delta\boldsymbol{q}^i(x) = \Delta\boldsymbol{q}^{i-1}(x) + \boldsymbol{f}_s^{i-1}(x)\left\{\boldsymbol{b}(x)\Delta\boldsymbol{P}^i - \Delta\boldsymbol{p}[\Delta\boldsymbol{q}^{i-1}(x)]\right\}\,. \tag{17}$$

The element theory and the equilibrium-based approach described above have been presented and discussed in more detail in Petrangeli and Ciampi [1997]. The algebraic expressions used for the fibre consitutive laws for concrete and steel can be found in Petrangeli [1996].

The equilibrium-based algorithm discussed above has been already implemented in the flexural fibre element by the authors where it has proven to be very efficient and robust. The implementation of this strategy into this new element with section shear modelling is, as shown above, very straightforward.

4. Truss Model for Shear Response

The truss idealisation (Fig. 5) has been widely used to evaluate the shear resisting mechanism proportions between concrete and transverse steel, incorporating the influence of axial load P. Watanabe and Ichinose [1991] suggested a method (for members with rectangular sections) to predict shear strength, where an estimate for the latter is obtained by using a superposition of a truss and an arch mechanism. A lower bound plasticity approach is used to limit the diagonal compression stress as a result of the combined truss and arch action. Ang *et al.* [1989] developed predictive shear equations after an extended analysis of circular bridge piers. A 45° truss mechanism is used to predict shear resistance provided by transverse steel. Recently, Priestley *et al.* [1994] indicated that shear strength can be predicted as a function of on three independent components: a concrete component dependent on ductility level, an axial load component resulting from the arch action, and a truss component dependent on the amount of transverse reinforcement.

In these models the angle θ of inclination of the diagonal cracks, to be used in the truss component, is considered independent of the applied lateral load. Following this common assumption, a truss model will be used herein only to define the 'pure' shear behaviour of a beam segment under monotonic loading. The axial load effect

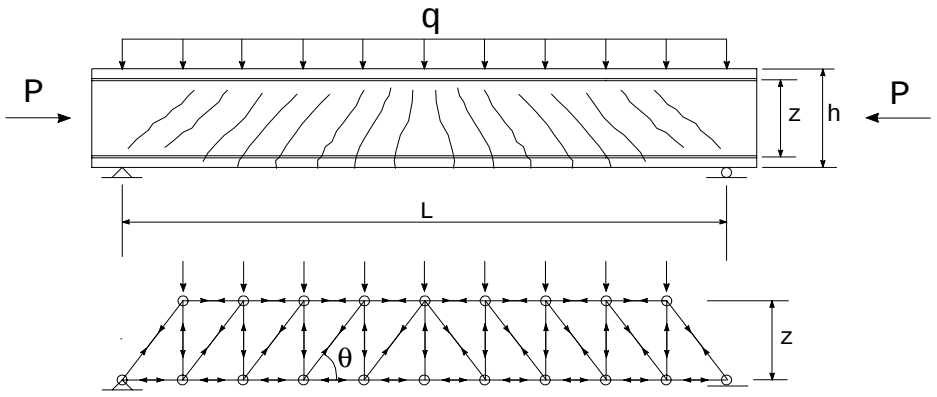

Fig. 5. RC beam truss idealisation.

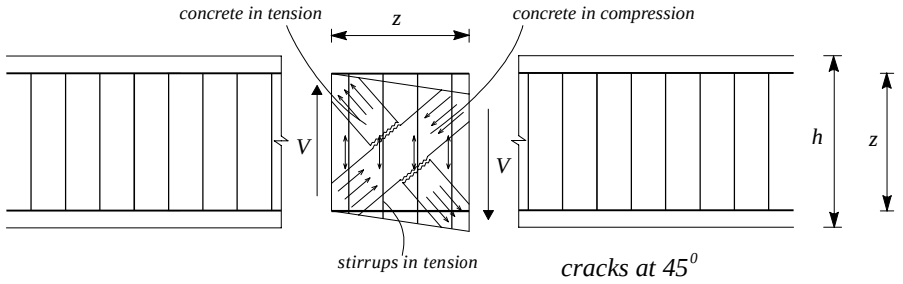

(a)

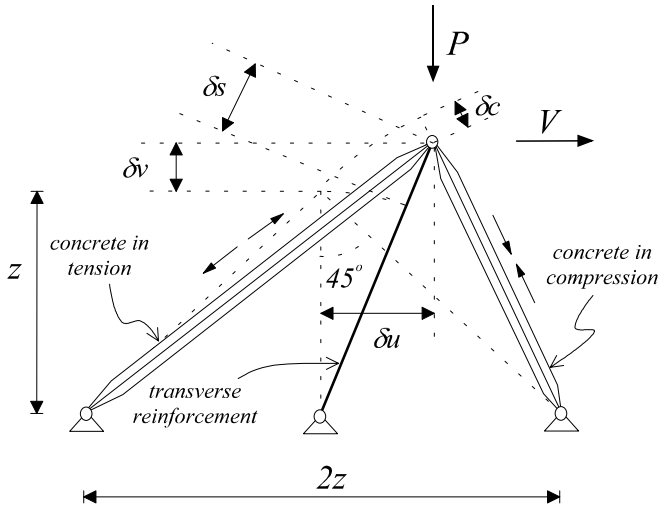

(b)

Fig. 6. Beam segment truss idealisation.

will be incorporated in the truss analogy so as to include its influence on concrete behaviour in both tension and compression.

The truss analogy used for the identification of the monotonic shear response is shown in Fig. 6. This model provides the shear force/shear deformation curve as a function of the applied axial load P, the shear reinforcement and the behaviour of concrete in the diagonal struts. The structural configuration shown in Fig. 6(b) is a representation of the beam segment depicted in Fig. 6(a). The following assumptions have been made in order to realise this simplified representation:

(1) The angle θ of inclination of the diagonal cracks has been assumed equal to 45° because this choice is very commonly adopted and provides good agreement with the experimental values in most cases.
(2) Concrete struts in compression (or in tension) present in the analysed segment are identified by a single truss element, whose cross-sectional area is a fraction

of the section gross area, depending on the position of neutral axis at flexural cracking point.

(3) The segment shear reinforcement is represented by an equivalent chord, whose cross-sectional area is equal to the sum of the transverse bars areas along the segment length and a fraction of the area of the longitudinal reinforcing bars equal to 0.3% of the section gross area. This latter contribution accounts for the effect of the longitudinal reinforcement on the shear resistance due to flexural compression in concrete and dowell mechanism.

(4) The chord stress-strain constitutive relations adopted are the same used for the fibres in the flexural analysis (the qualitative behaviour is shown in Fig. 1, details are given in Petrangeli [1996]).

Assumption (1) will determine the representative segment length. This will be such that a complete 45° compression strut will be included [see Fig. 6(a)]. The value of 45° can be replaced with 30° (as suggested in Priestley *et al.* [1994]) or other consistent values, depending on element geometry. Assumption (2) requires an estimate the position of neutral axis at cracking point (i.e. using a moment-curvature analysis) to evaluate the section compression zone.

Even though the location of equivalent struts might appear incorrect because the axial force P is parallel to the transverse steel, the proposed system configuration is capable of reproducing the correct sequence of damage phenomena occuring for increasing applied shear force values. At early stages ($V < V_{\rm cr}$ = cracking shear) the shear force is completely carried by the concrete struts. Deformations in the steel chord do not take place until the tension concrete chord fails. Once the tension chord has failed, the resisting mechanism rests on the steel and on the compressive concrete strut only. Subsequently, failure will be reached by either concrete failure in compression or yielding of transverse steel.

The $V-\gamma$ curve, representative of the segment behaviour, is obtained by applying the force V by small subsequent increments $\Delta V(i)$ up to failure. The distortion γ can be defined as $\delta u/(z+\delta v)(\cong \delta u/z)$. In Fig. 6(b), deformation of the compressive concrete strut δc and that of the transverse steel δs are indicated. With this model, the ultimate state of the system (i.e. the achievement of either steel or concrete ultimate strain, whichever occurs first) can easily be related to the cross-section geometry, the material properties and the applied axial load. Concrete will generally dominate the behaviour when a high axial load is applied. Steel will dominate instead in the case of low axial load or insufficient transverse reinforcement.

The above described procedure will provide a discrete relation in the following form:

$$V(i) = f(\gamma(i))\,, \tag{18}$$

where i is the generic applied load step. Typical examples of such curves are showed in Fig. 7. The discrete relation (18) will be interpolated with the following function:

$$V(\gamma) = K_1 \ \arctan(K_2\gamma) \tag{19}$$

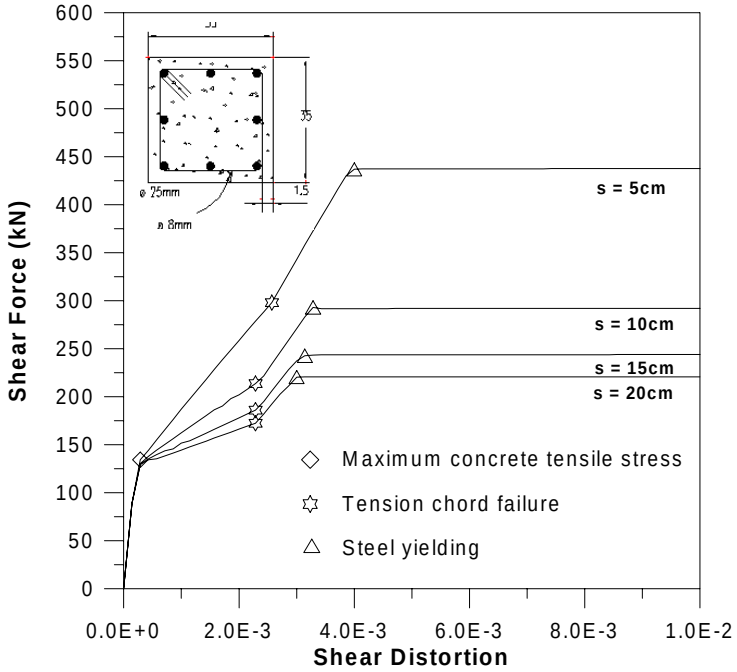

(a)

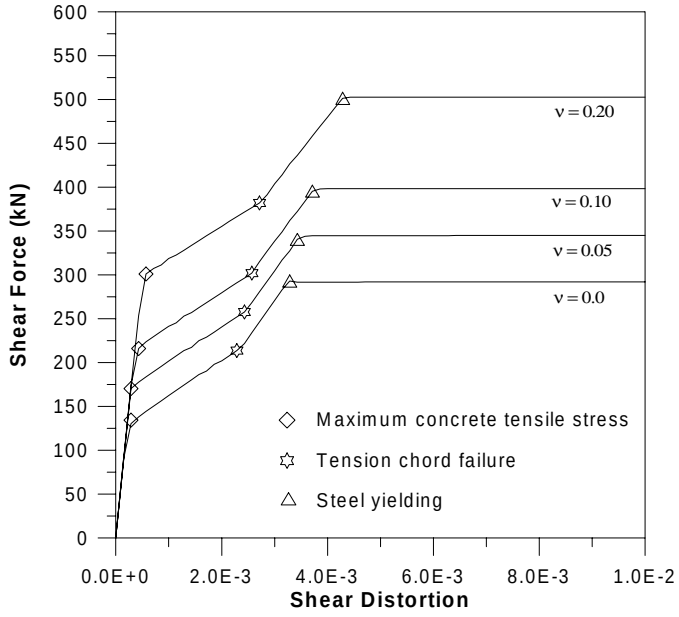

(b)

Fig. 7. Truss model response.

where the two scalar parameters K_1 and K_2 are obtained as follows:

$$K_1, K_2 : \{V(\gamma(i)) - V(i)\}^2 = \min . \tag{20}$$

In (20) the least square minimization criterion has been adopted. Other interpolation schemes can be used to better define the primary curve. Here expression (19) has been proposed because it is an odd function, consistent with the hypothesis of symmetric response in both directions of load application. The parameter K_1 acts as a 'curve amplitude factor' and K_2 as a 'shape factor'. The product $K_1 K_2$ gives the initial elastic shear stiffness.

In Fig. 7 several examples of the truss model response are presented. The analysed section is shown on top of Fig. 7(a) (dimensions in cm) together with the position of longitudinal reinforcing bars, in order to identify the relative segment size. Specimens have an aspect ratio of 2.5, a concrete compressive strength of 35 MPa, a tensile strength of 2.95 MPa and transverse steel yield stress of 450 MPa. The $V-\gamma$ curves have been plotted up to a distortion of 0.01. The symbols identify the force values at which the tensile strength is reached in the concrete tension chord, the force values at which the concrete tension chord fails after the material softening phase, and the force values at which yielding is reached in the steel chord (note that the softening branch in the tensile part of the concrete constitutive relation can be manipulated, for a realistic description, as a function of the concrete fracture energy [Petrangeli, 1996]). In Fig. 7(a) the segment is analysed for four different stirrups spacings without axial load, in Fig. 7(b) four different values of axial load have been considered for a constant stirrup spacing $s = 10$ cm. Indicated in Fig. 7(a) are the considered stirrup spacings, and in 7(b) the axial load ratios $\nu = P/f'_c A_g$. The axial load governs the behaviour of concrete in tension. In the case of high compression the uncracked stiffness is mantained up to very high values of shear force (more than 50% of maximum strength). None of these cases showed concrete failure in compression before stirrups yielding. As a matter of fact the model tends to underestimate compression in the concrete strut since it ignores the component due to bending.

A summary of the maximum strengths found with the sectional truss analogy is reported in the following. In the same table the shear strengths found using the Priestley's formulae (for curvature ductility $\mu_\phi = 0$) is reported.

Axial load ratio 0.0			Stirrups spacing 10 cm		
Stirrups spacing	Priestley *et al.*	Truss	Ax. load ratio	Priestley *et al.*	Truss
20 cm	242 kN	222 kN	0	314 kN	293 kN
15 cm	266 kN	244 kN	0.05	342 kN	344 kN
10 cm	314 kN	293 kN	0.1	371 kN	399 kN
5 cm	459 kN	438 kN	0.2	428 kN	504 kN

The increase of transverse reinforcement obviously produces the same influence on the value of the maximum strength in both models, since the same truss configuration is adopted. The sectional truss model was shown to be more sensitive to the increase of axial load.

The described model gives an estimate of the 'pure shear' behaviour, it does not incorporate the influence of flexural ductility. In the next section, the expression (19) will be manipulated by letting K_1 become a function of axial deformation; as a consequence, the influence of ductility on shear behaviour will be taken into account by means of a varying 'curve amplitude factor' K_1 during cycling. By doing so, the primary curve will be used to define the skeleton branch of the section shear hysteretic relationship.

Although several models, calibrated to experimental results, have been proposed for the prediction of shear response [Ang *et al.*, 1989; Priestley *et al.*, 1994; Wakanabe and Ichinose, 1991], in this context a simplified phenomenological approach has been suggested to develop a consistent methodology to account for concrete cracking effects on RC beams in both flexural and shear behaviour. In fact, it is not trivial to note again that the same uniaxial constitutive relation was used to model longitudinal concrete fibres and diagonal struts.

5. Section Shear Hysteretic Stress-Strain Relationship

The equations defining the skeleton branch (cyclic response envelope), unloading and reloading branches together with the rules adopted for cycling are described in the following (see also Fig. 8). First the skeleton branch and the damage criterion will be discussed, then the construction of unloading and reloading paths.

In defining the $V - \gamma$ primary curve (in Sec. 3), shear strength dependence on ductility level has thus far been neglected. The skeleton branch of the hysteretic

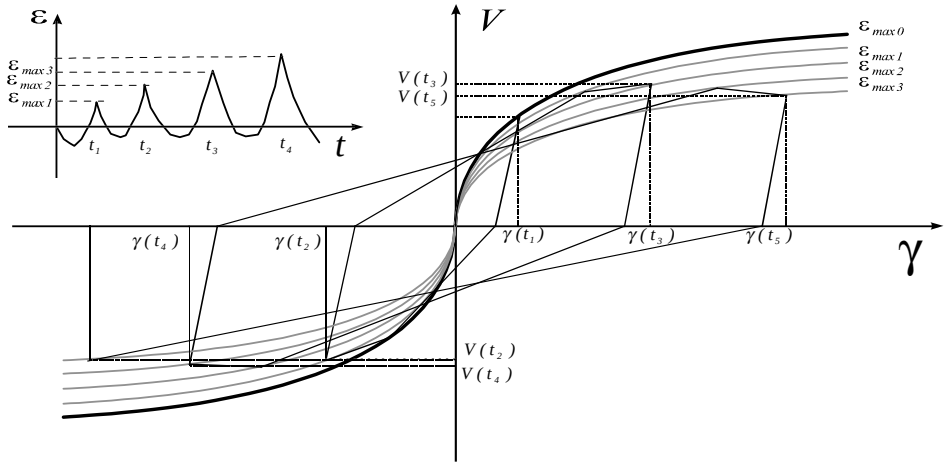

Fig. 8. Section shear hysteretic model.

relationship (which defines the loading branches in the cyclic analysis) will instead incorporate a degradation criterion where the primary curve is a function of section axial deformation ε. As mentioned above, this latter has been chosen to be the damage indicator because it gives an average value of the axial deformation over the section, and is therefore related to the crack opening.

In fact, the relation between curvature and axial elongation in reinforced concrete sections can be accurately reproduced by a fibre section using realistic constitutive behaviour as in our case. It is well known, although often ignored, that sections elongate under bending due to the shifting of the neutral axis. This elongation (rocketing) is proportional to the section curvature but depends also on the longitudinal reinforcement ratio and on the axial load. Therefore, the centroidal axial deformation ε provides a useful indicator of all the above-mentioned components which have an influence on the section shear strength.

Assuming a linear relation between shear strength and flexural damage, the equation of the shear skeleton branch can be expressed, in the most general form, as follows:

$$V = (K_{10} - \varepsilon_{\max} m)\ \arctan(K_2 \gamma)\,, \quad \varepsilon_0 \leq \varepsilon_{\max} \leq \varepsilon^* \tag{21}$$

where K_{10} is the value of K_1 found with the truss analysis, corresponding to the shape of the primary skeleton curve ($\varepsilon_{\max} = 0$ in Fig. 8), $\varepsilon_{\max}$ are the maximum values of positive axial deformation recorded during cycling, m is a coefficient defining the slope of the $V - \varepsilon_{\max}$ relation (shown in Fig. 9), ε_0 and ε^* are two axial deformation values defining the shear strength degradation interval. Indications on these three latter parameters can be assumed based on Priestley *et al.* [1994] model and considerations on the allowable crack opening.

Degradation does not take place until axial deformation exceeds ε_0:

$$V = K_{10}\ \arctan(K_2 \gamma)\,, \quad \varepsilon_{\max} < \varepsilon 0 \tag{22}$$

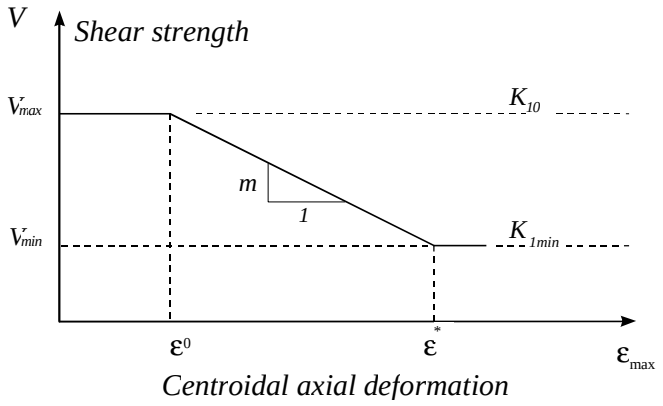

Fig. 9. Damage criterion.

If damage development leads to an axial deformation greater than a specified value ε^* (see Fig. 9), Eq. (21) becomes:

$$V = K_{1\,\min}\ \arctan(K_2\gamma)\,, \quad \varepsilon_{\max} > \varepsilon^* \tag{23}$$

It can be argued that the linear experimental correlation between concrete contribution to shear strength and ductility (as suggested in Priestley *et al.* [1994]) might not remain the same between total shear strength and ductility. Nonetheless, given our interest in the qualitative description of this kind of problem, the linear correlation has been retained and used for the total section shear strength as well.

Figure 8 describes the mechanism according to which the skeleton branch is modified during cycling. A typical plot of axial deformation as a function of time is also provided for better understanding. The initial loading branch coincides with the primary curve, which corresponds to the undamaged condition where $\varepsilon_{\max} = 0$. When a positive value of axial deformation $\varepsilon_{\max 1}$ (greater than the specified ε_0) is reached, the loading branch becomes the one corresponding to Eq. (21) where $\varepsilon_{\max} = \varepsilon_{\max 1}$. When a new maximum value of $\varepsilon_{\max} = \varepsilon_{\max 2}$ is reached (e.g. after a load reversal), the skeleton branch will follow the new curve corresponding to $\varepsilon_{\max} = \varepsilon_{\max 2}$. Each time the crack opening exceeds the previous maximum value during cycling, the skeleton branch is subjected to a 'contraction', therefore both strength and stiffness degrade. If $\varepsilon_{\max}$ exceeds ε^*, the loading branch described by Eq. (23), is followed. This corresponds to the residual shear resisting behaviour.

Unloading branches follow linear paths having a slope defined by the user. By default the program assumes this slope to be equal to the initial stiffness. Two different slopes for the unloading branch can be specified, for shear force values greater or smaller than cracking shear $V_{\rm cr}$, as found with the truss analysis.

$$V_{unld.} = k_{in}\gamma \quad V > V_{\rm cr} \tag{24}$$

$$V_{unld.} = k_{in}k_{\rm cr}\gamma \quad V \leq V_{\rm cr} \tag{25}$$

where k_{in} is the initial shear stiffness which can be computed from the the first derivative of Eq. (21) evaluated in $\gamma = 0$:

$$k_{in} = \left(\frac{\partial V}{\partial \gamma}\right)_{\gamma=0} = K_{10}K_2 \tag{26}$$

and $k_{\rm cr} < 1$ is a coefficient defining the cracked shear stiffness.

When a load reversal occurs, the latest point (V_{lst}, γ_{lst}) is recorded and compared with the point corresponding to maximum absolute value of distortion reached in previous steps ($V_{\max}$, $\gamma_{\max}$). The linear unloading path defined by Eqs. (25) or (26) is then followed. When the horizontal axis is reached during an unloading branch, the slope of the following transition (or reloading) branch is computed based on the position of the point ($-V_{\max}$, $-\gamma_{\max}$). If a reversal occurs during an unloading branch, the latter is followed in the opposite direction up to (V_{lst}, γ_{lst}). Typical

cycles are shown in Fig. 8. Loading follows the undamaged curve from the origin up to (V_1, γ_1), where a load reversal occurs. An unloading branch [with initial stiffness, Eq. (24)] is followed down to the horizontal axis. The subsequent transition branch goes to ($-V_1$, $-\gamma_1$). While load increases from $-V_1$ to $-V_2$, the axial deformation changes from 0 to $\varepsilon_{1\max}$ and the skeleton branch changes gradually from $\varepsilon_{\max} = 0$ to $\varepsilon_{\max} = \varepsilon_{\max 1}$. When ($-V_2$, $-\gamma_2$) is reached, a new reversal occurs and after the unloading path, the transition branch goes to (V_2, γ_2). Analogous rules are followed for subsequent cycles.

The model can be considered a modified Takeda, in which the classic bilinear skeleton is replaced with a continuous curve which can be scaled depending on the ductility level reached during the analysis.

6. Numerical Verifications

A large number of cyclic static and dynamic numerical tests on simple structures have been performed to examine the element behaviour. In Fig. 10 the cross-section of a pier tested by the European Laboratory for Structural Assessment (ELSA) is presented along with the reinforcement details (see also Pinto *et al.* [1995] for

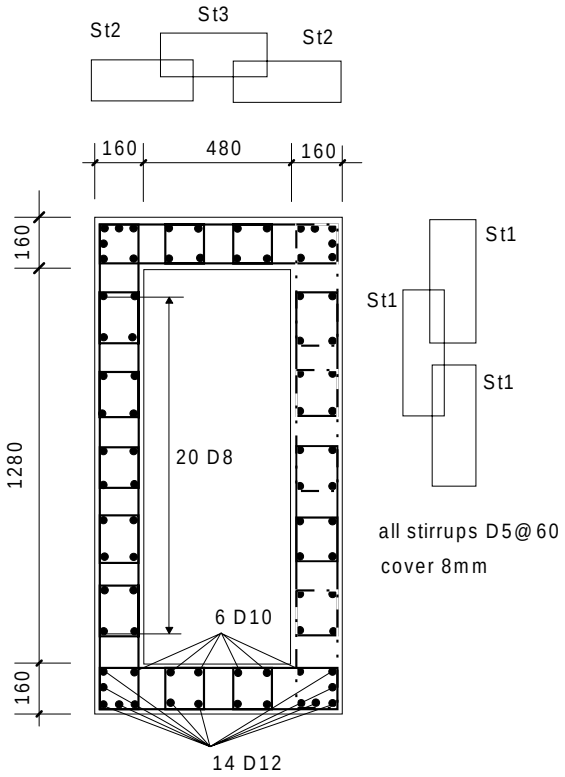

Fig. 10. ELSA pier section.

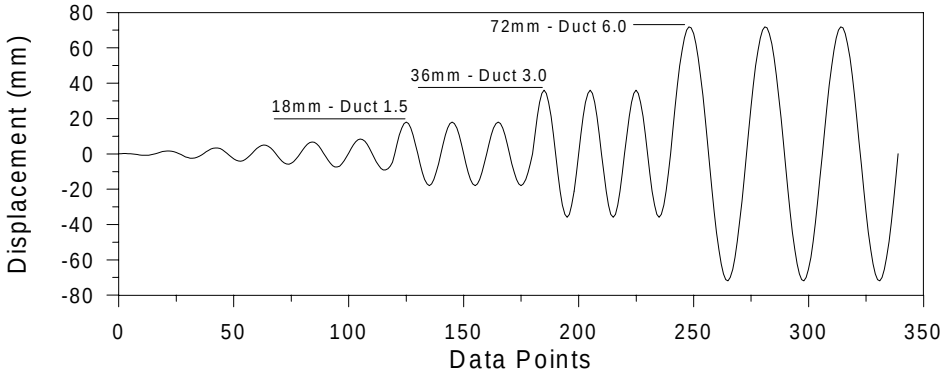

Fig. 11. ELSA imposed displacement path.

more details). The cyclic quasi-static test performed with the application of the transverse displacement path shown in Fig. 11, has been selected for the numerical verification. The pier has a particulary low shear span ratio (1.75). Axial load is applied in a mixed mode with a vertical actuator and four prestressing rebars placed at the four section corners, with a non-dimensional ratio $P/f'_cA_g = 0.1$. The pier has been designed using the Eurocode 8 [EC8, 1994] design recommentations and, despite the extremely low shear span ratio, it exhibits ductile characteristics.

The pier has been analysed using only one element with 5 Gauss points. Two analyses have been conducted in parallel. The first, performed with the classic fibre element without shear modelling, shows that energy dissipation was overestimated due to an eccessive value of base curvature prediction .The second, using the new element with shear modelling, predicts the transverse displacement profile with more accuracy, as shown in Fig. 12.

For this type of structural member with low shear span ratio, the classic fibre element prediction seems to be rather inadequate for assessing the distribution of the longitudinal strains along the element length. Better results are obtained with the proposed model which shows a distribution of shear distortions along the element length proportional to curvature and axial strain. The model is therefore capable of reproducing the localisation of bending and shear distortion at the column base, as seen in Fig. 13.

A comparison of the force-displacement hysteresis loops for the purely flexural and the new model are shown in Figs. 14(a)–(b). The experimental behaviour shows very smooth transition branches, well reproduced only when taking into account the shear behaviour. The classic flexural model instead presents a well-defined pinching effect, which does not seem to be realistic. The stiffness given by the purely flexural model is larger than the experimental one since the shear flexibility is ignored, especially when, due to diagonal cracking, this flexibility becomes comparable to the flexural one.

Fibre Element Without Shear

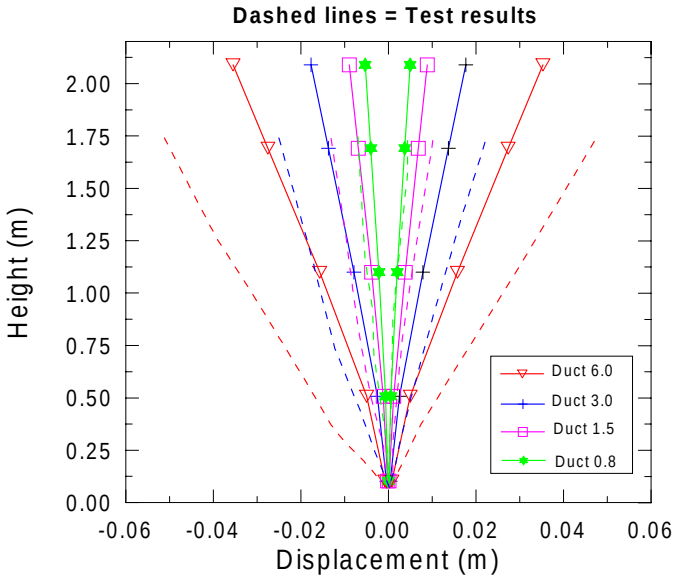

Fibre Element With Shear

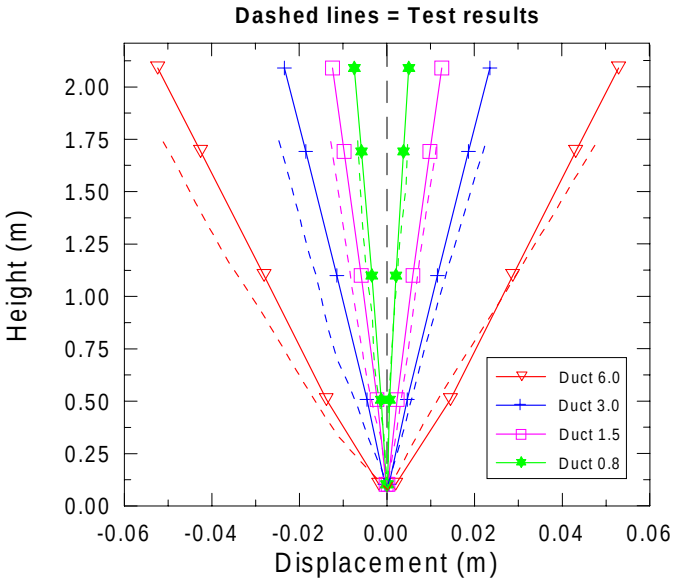

Fig. 12. ELSA — Lateral displacement profiles.

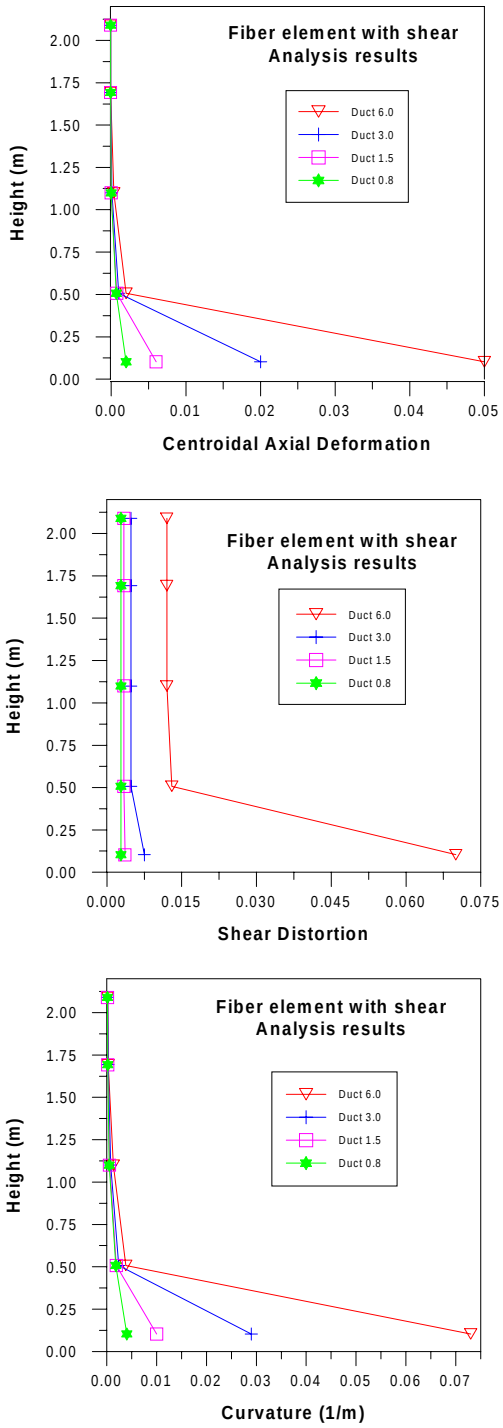

Fig. 13. ELSA — Deformations along the pier.

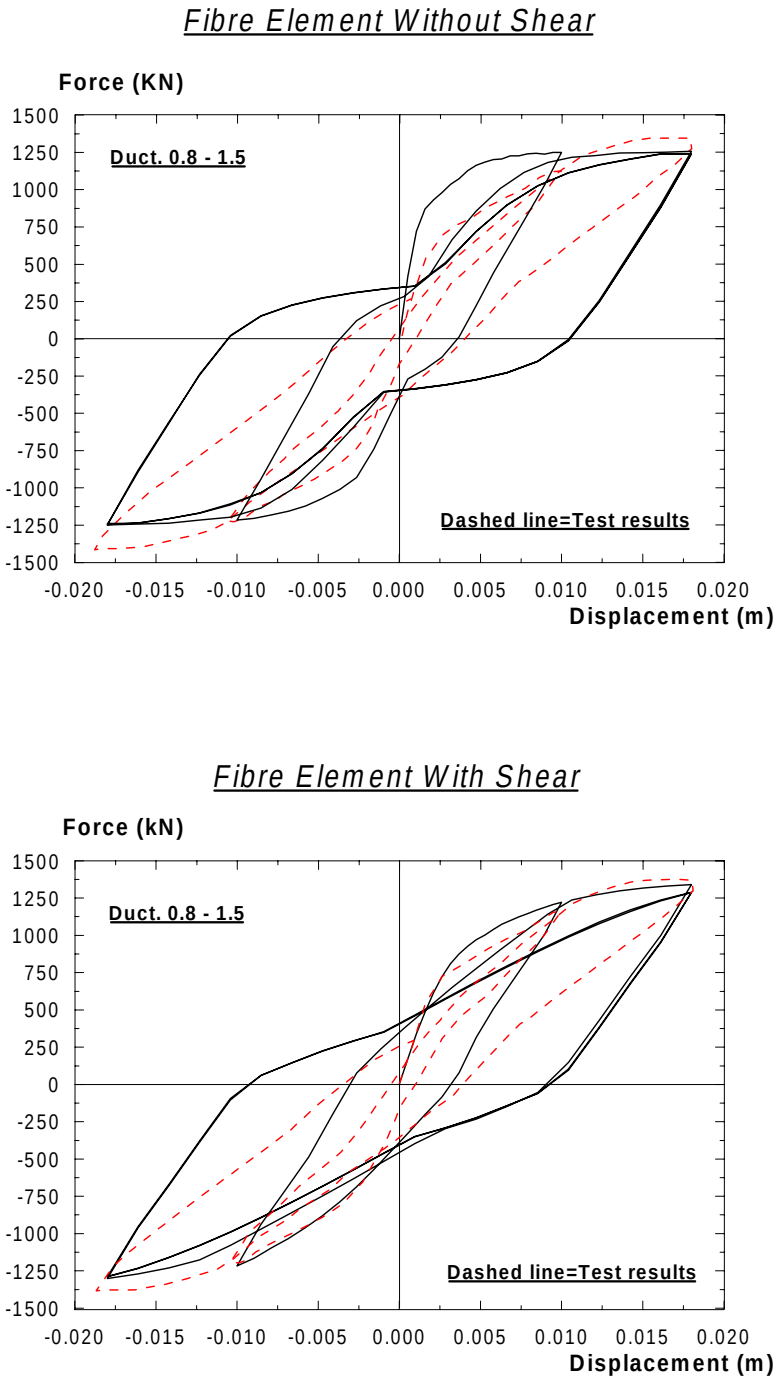

(a)

Fig. 14. ELSA force-displacement response.

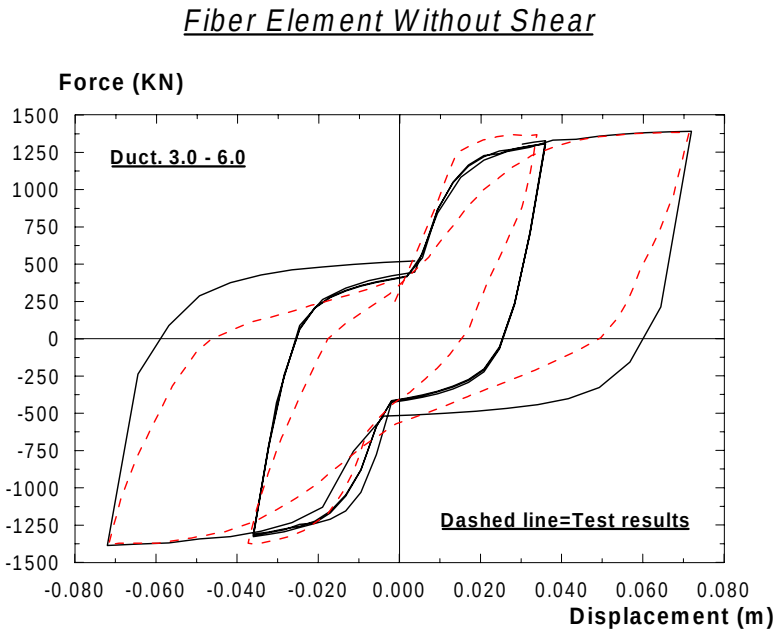

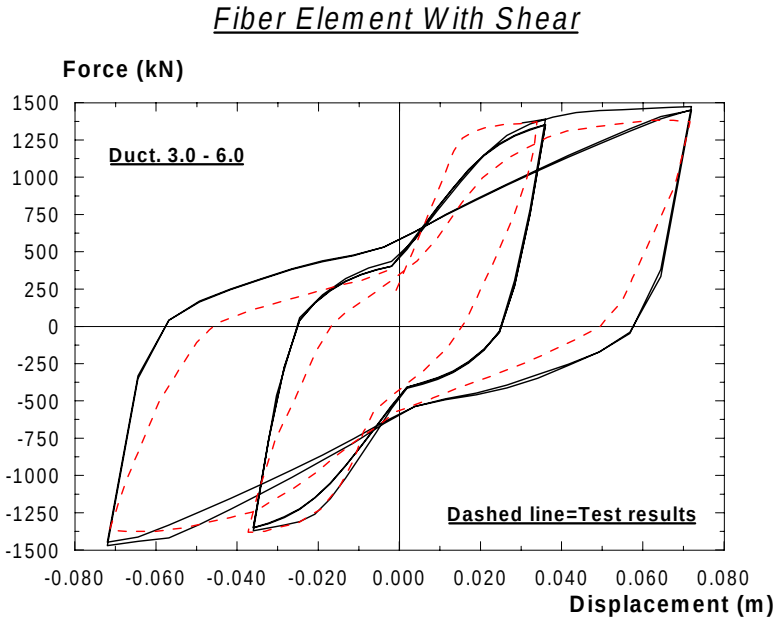

(b)

Fig. 14. (*Continued*)

In the second numerical example, a one-storey one-bay frame is considered. Column height is 3 m, while beam length is 6 m. Column section is 75×75 cm (longitudinal reinforcement $r_s = 2\%$), beam section is 56.5×100 cm ($r_s = 1.5\%$). Two masses of $100t$ have been lumped at node locations and the structure has been subjected to the El Centro N-S acceleration record ($PGA = 0.34\ g$). The purpose of the present example is to show the response of redundant structures, where significant stress and strain redistributions occur due to coupled bending and shear non-linear behaviours. The selected column height/beam length ratio will enforce a significant shear demand in columns, while the beam should behave essentially elastically. Again, two analyses were conducted in parallel with the classic fibre element and with the element including the shear behaviour.

As expected, the beam horizontal displacement time histories [Fig. 15(a)] show that, including the shear deformation, a much greater peak displacement is predicted. When inelastic shear distortions occur in columns, a significant change in structure period is observed, consequently the two time histories present a large phase difference. As shown in Figs. 15(b)–(c), large shear deformations and strength degradation occur in columns, not in the beam. Figures 15(d) and 15(f) (showing flexural hysteresis loops at the column base) indicate that in both cases the same level of ductility is reached. Instead, in Figs. 15(e) and 15(g) it can be noted that the flexural model largely overestimates energy dissipation in the beam. Moreover, the fibre element with shear shows that flexural damage occurs first, then, as a consequence of concrete damage, large shear distortions occur. From then on, column moment/curvature cycles are very narrow, indicating that only a little more flexural energy can be dissipated.

The example shows that, although the model is approximate and cannot capture the real failure mechanism in shear, nonetheless the introduction of shear deformability can yield substantial differences on structural behaviour.

The third and final example presents the analysis of a circular bridge pier with particularly low shear reinforcement ratio ($\rho_s = 0.09\%$). The pier was tested under pseudo-static cyclic lateral loading with a cantilever scheme (aspect ratio = 2.0) and exhibited a brittle behaviour (see Benzoni *et al.* [1996]). In this case the shear evolution relationship is not capable of reproducing the post-failure behaviour, but the finite element correctly predicts the cyclic behaviour up to failure, indicating shear and flexural contribution to displacement with satisfactory accuracy. The displacement at which failure is expected to occur (marked with a triangle in Fig. 16(a) can be predicted based on the shear distortion at strirrups yield found with the truss analysis. The numerical results show good agreement with the experimental evidence (Fig. 16).

Also in this case the element response has been compared with the response of the flexural element [Fig. 16(b)]. Again, the new element predicts with more accuracy the amount of energy dissipation and the displaced shape. The maximum curvature at column base predicted with the flexural model is almost three times the experimental one. The new element instead predicts with good accuracy

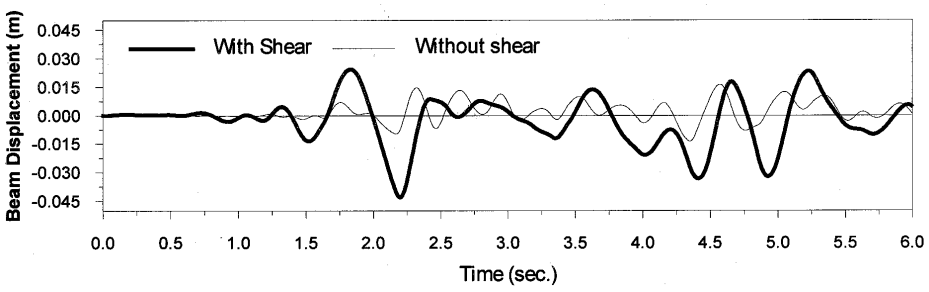

(a)

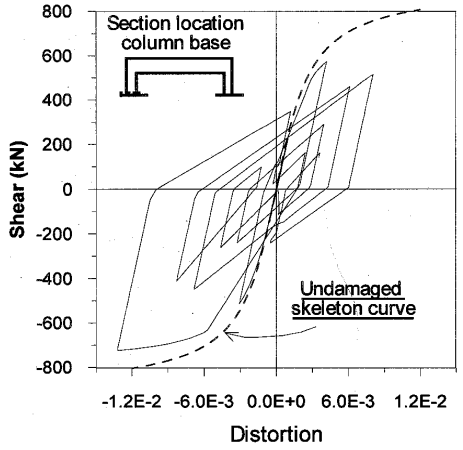

(b)

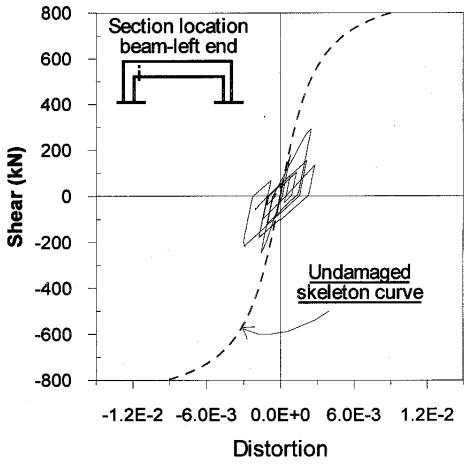

(c)

Fig. 15. One-storey frame seismic analysis.

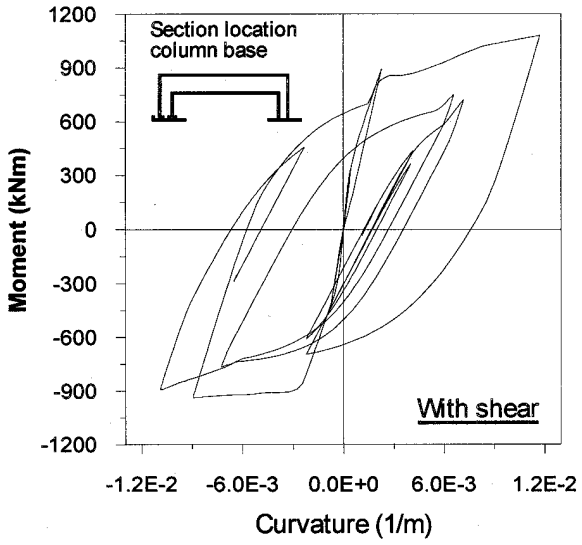

(d)

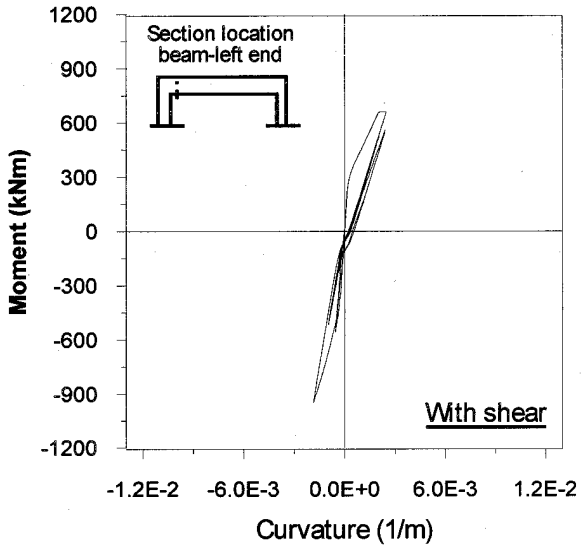

(e)

Fig. 15. (*Continued*)

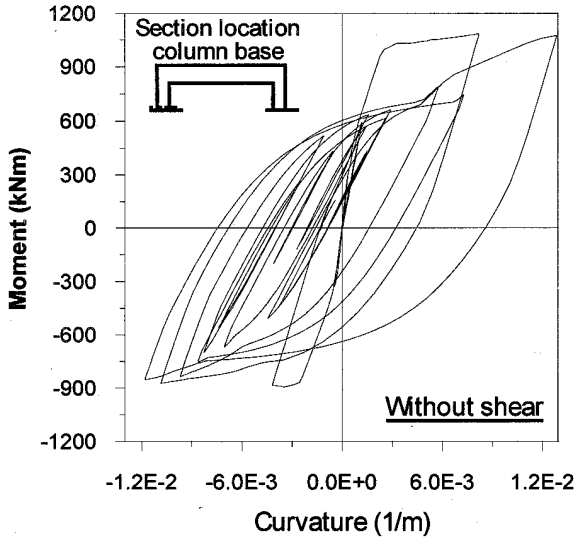

(f)

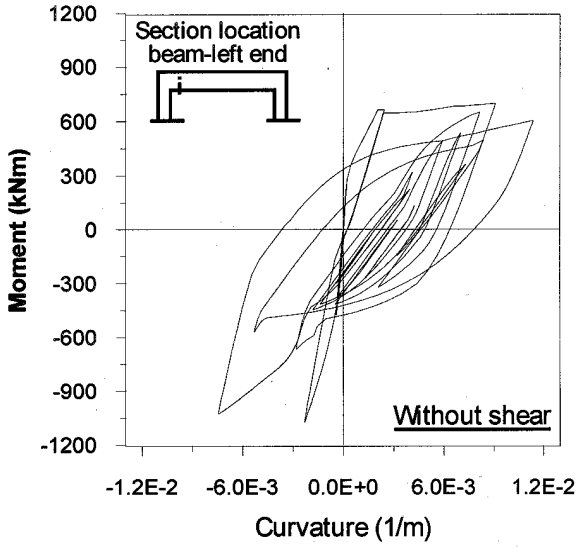

(g)

Fig. 15. (*Continued*)

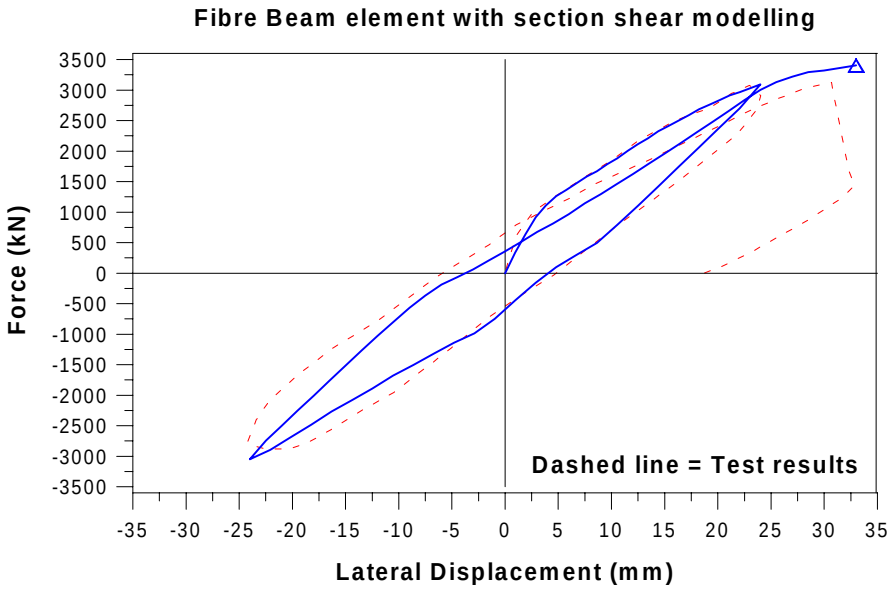

(a)

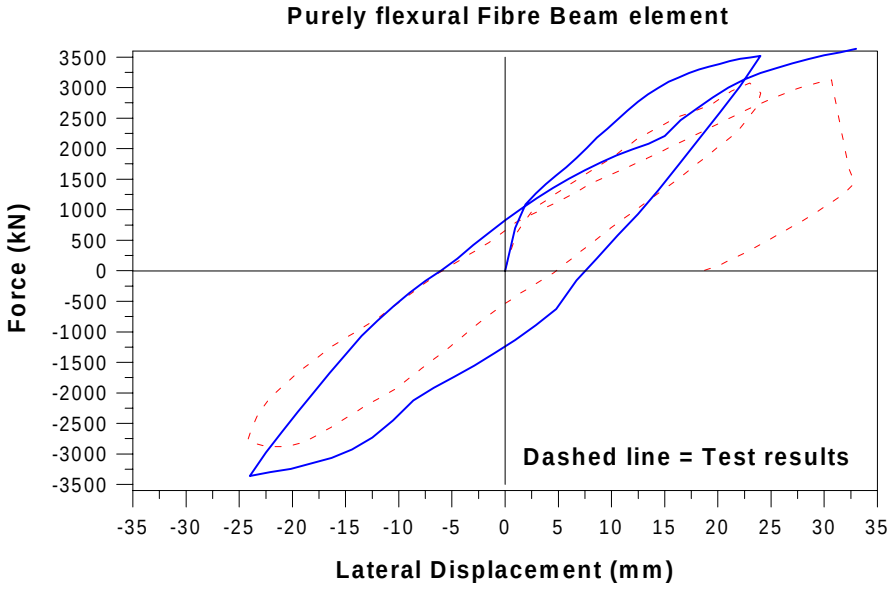

(b)

Fig. 16. Full scale bridge pier test.

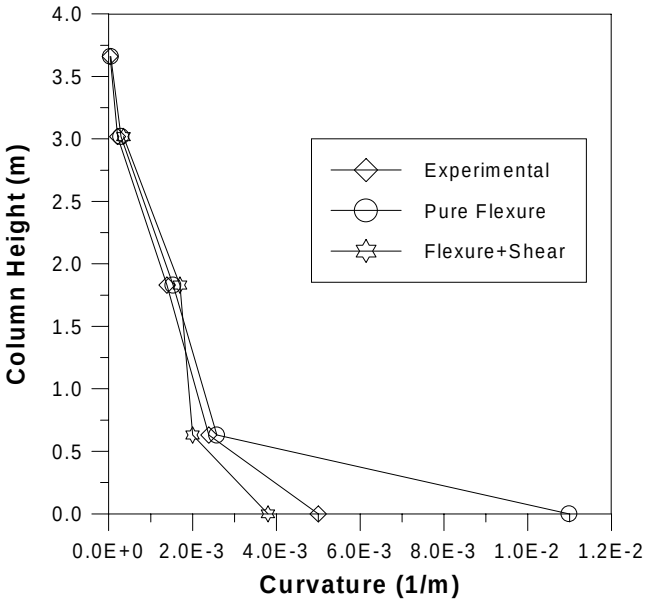

(c)

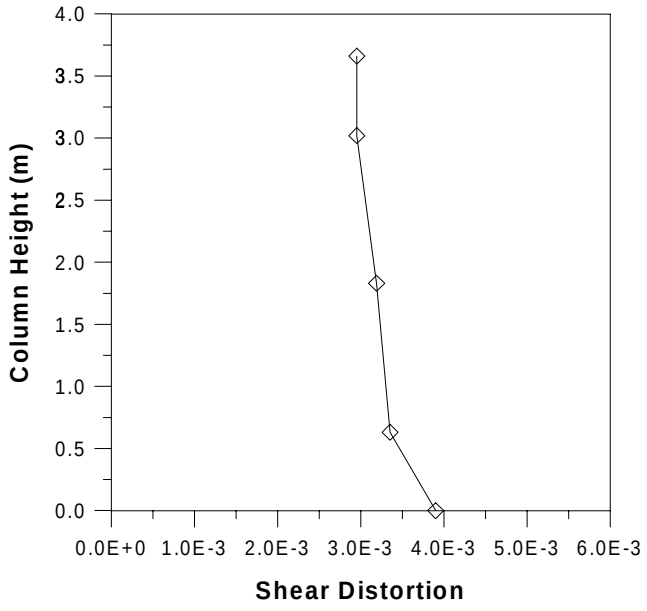

(d)

Fig. 16. (*Continued*)

the base curvature, thus giving a correct distribution along the pier [Fig. 16(c)]. The distribution of shear distortions at expected failure is shown in Fig. 16(d).

Two extreme cases of very ductile and very brittle shear sensitive bridge pier behaviours have been presented with the purpose of investigating the element behaviour in a wide range of structural configurations. Substantial differences with state-of-the-art beam elements encourage further effort in the development of models including shear capabilities.

7. Conclusions

This paper is considered as a first attempt to solve the moment-shear-axial force interaction in reinforced concrete beam-column elements using the finite element method. At this stage a simplified section shear behaviour has been introduced into a state-of-the-art fibre beam element.

With the bending-shear hysteretic coupling being a function of local damage, the distributed inelasticity member model adopted gives the possibility of predicting the correct deflected shape and evaluating the displacement contributions due to shear and bending along the element length with satisfactory accuracy. The idea of superposing different types of theories to describe the interaction seems to be effective in finding out the essential aspects for further studies. The procedure has been implemented in the framework of an equilibrium-based formulation for the non-linear beam element, which proved to be robust and completely reliable for computational purpose.

The primary skeleton curve of the hysteretic shear relationship has been calibrated using a non-linear truss model, composed of a simple three-chord strut-and-tie configuration. More complex hysteresis rules, for example the ones presented in Ozcebe and Saatcioglu [1989], incorporating pinching effect and other relevant observed phenomena, could be easily implemented to better describe the cyclic shear behaviour. Implementation of a more complex shear constitutive behaviour does not require modification to the element structure.

A simplified damage criterion for the bending-shear interaction has been proposed based on recent models developed from a large number of experimental observations [Priestley *et al.*, 1994]. The linear dependence of shear capacities on section ductility provides a non-linear distribution of shear deformations along the element length. As a consequence, the γ distribution will reflect that of longitudinal axial strains, which seems to be accurate enough to predict the correct deformed shape. Again, further refinement of this bending-shear interaction mechanism could be sought, although a definite step forward in the understanding of this mechanism can only be obtained with a full three-dimensional modelling of the local concrete behaviour along the element. A fibre beam element with shear modelling using three-dimensional constitutive behaviour for the concrete fibres, has been recently implemented in Petrangeli [1996], Petrangeli *et al.* [1997] and Petrangeli and Pinto [1997]. The numerical examples presented show however, that an adequate

description of the interaction between flexural and shear capacities can be obtained by the present simpler model, although limited information is obtained on the post-peak behaviour in brittle shear failures.

Symbols

M_x, M_y = bending moment about x and y-axes
γ = shear distrortion
χ = section curvature
ε = section axial deformation
$\varepsilon_{\max}$ = maximum values of axial deformation
$\boldsymbol{p}(x)$ = section stress vector
$\boldsymbol{q}(x)$ = section strain vector
$\boldsymbol{k}_s(x)$ = section stiffness matrix
$\boldsymbol{f}_s(x)$ = section flexibility matrix
$\alpha(x)$ = shape function matrix
$\boldsymbol{b}(x)$ = stress shape functions matrix
$\boldsymbol{K}$ = element stiffness matrix
$\boldsymbol{F}$ = element flexibility matrix
$\mathbf{P}$ = element nodal force vector
$\mathbf{Q}$ = element nodal displacement vector
$\boldsymbol{r}_p(x)$ = section residual force vector
K_1 = shear model parameter
K_2 = shear model parameter
μ_ϕ = curvature ductility
ν = normalised axial load
f'_c = concrete compressive strength
A_g = section gross area
m = degrading stiffness parameter
$k_{\rm cr}$ = shear model cracking parameter
k_{in} = initial shear stiffness
M_i, M_j = element nodal bendings
P_j = element axial load
θ = diagonal crack inclination angle
$V_{\rm cr}$ = cracking shear value
ρ_s = percentage of transverse reinforcement
r_s = percentage of longitudinal reinforcement

References

ACI [1989] ACI 318/89 — *Building Code Requirements for Reinforced Concrete Structures*, American Concrete Institute, Detroit, Michigan.

Ang, B. G., Priestley, M. J. N., Paulay, T. [1989] — "Seismic shear strength of circular reinforced concrete columns," *ACI Structural Journal* **86** (1), 45–59.

ATC-6 [1981] Applied Technology Council. *Seismic Design Guidelines for Highway Bridges* (Berkeley, California).

Bazant, Z. and Bhat, P. D. [1977] "Prediction of hysteresis of reinforced concrete members," *J. Struct. Engrg.* ASCE **103**, 153–166.

Benzoni, G., Ohtaki, T. and Priestley, M. J. N [1996] *Seismic Performance of Full Scale Bridge Column — As Built and As Repaired* (Univeristy of California San Diego, SSRP 96/04).

Collins, M. P. [1978] "Towards a rational theory for reinforced concrete members in shear," *Proceedings ASCE*, Vol. 104, No. ST4.

EC8 [1994] Eurocode 8. *Design Provisions for Earthquake Resistance of Structures*, ENV 1993-2, Comite European de Normalization, Brussells.

Garstka, B., Kratzig, W. B. and Stangenberg, F. [1993] "*Damage assessment in cyclically loaded reinforced concrete members*," in *Structural Dynamics, EURODYN '93*, Moan Ed. (Balkema, Rotterdam), Vol. 1, pp. 121–128.

Kaba, S. A. and Mahin, S. A. [1984] *Refined Modelling of Reinforced Concrete Columns for Seismic Analyses.* University of California at Berkeley, Earthquake Engineering Research Center report 84/03.

Mahasuverachi, M. and Powell, G. H. [1982] *Inelastic Analysis of Piping and Tubular Structures.* University of California at Berkeley, Earthquake Engineering Research Center report 82/27.

Minami, K. and Wakabayashi, M. [1981] "Rational analysis of reinforced concrete columns," in IABSE Colloquium on 'Advanced Mechanics of Reinforced Concrete', Delft 1981.

Ozcebe, G. and Saatcioglu, M. [1989] "Hysteretic shear model for reinforced concrete members," *J. Struct. Engrg.* ASCE **115**.

Petrangeli, M. [1996] "Modelli numerici per strutture monodimensionali in cemento armato," Dissertation, University of Rome "La Sapienza", Italy.

Petrangeli, M. and Ciampi, V. [1997]. "Equilibrium based numerical solutions for the nonliner beam problem," *Int. J. Num. Mets. in Engrg.* **40**, 423–437.

Petrangeli, M. Pinto, P. E. and Ciampi, V. [1997] "Towards a formulation of a fibre model for elements under cyclic bending and shear," *Proc. Fifth SEDEC Conference on European Seismic Design Practice*, Chester (UK), Oct. 1995 (Ed. Balkema, Rotterdam).

Petrangeli, M. and Pinto, P. E. [1997] "Finite element modelling of the Hanshin viaduct failure in Kobe," *Proc. second Italy-Japan Workshop on Seismic Design and Retrofit of Bridges*, Rome, Feb. 1997.

Pinto, A. V., Verzeletti, G., Negro, P. and Guedes, J. [1995] "Cyclic testing of a squat bridge pier," in European Laboratory for Structural Assessment , Report EUR 16247 EN.

Priestley, M. J. N., Verma, R. and Xiao, Y. [1994] "Seismic shear strength of reinforced concrete columns," *J. Struct. Engrg.* ASCE **120**.

Priestley, M. J. N., Seible, F., Verma, R. and Xiao, Y. [1993] *Seismic Shear Strength of Reinforced Columns*, University of California san Diego, SSRP 93/06.

Sfakianakis, M. G. and Fardis, M. N. [1991] "RC column model for inelastic seismic response analysis in 3D," *J. Struct. Engrg.* ASCE **117**.

Spacone, E., Ciampi, V. and Filippou, F.C. [1992] *A Beam Element for Seismic Damage Analysis*, University of California at Berkeley, Earthquake Engineering Research Center report 92/08.

UBC [1988] Uniform Building Code, International Conference of Building Officials, Whittier, California, USA.

Watanabe, F. and Ichinose, T. [1991] "Strength and ductility design of RC members subjected to combined bending and shear," *Proc. Workshop on Concrete Shear in Earthquake*, University of Houston, Texas, pp. 429–438.

Yang, B. L., Dafalias, Y. F. and Herrmann, L. R. [1985] "A bounding surface plasticity model for concrete," *J. Engrg. Mechanics*, ASCE **111**.